

MULTI-ZONE MODELING AND SIMULATION OF INDUSTRIAL LARGE-LENGTH CONTINUOUS FURNACES FOR BRICK PRODUCTION

Spyros Mourtzoukos, Stamatis Manesis

University of Patras
Electrical & Computer Engineering Dept.
Patras 26500, Greece

stam.manesis@ece.upatras.gr

Abstract

The dynamic behavior of an industrial tunnel-type furnace is of the fundamental importance for the quality of the processed products. The knowledge of the furnace dynamics can make the control of the system easier as well as it can eliminate certain operational problems. The various subsystems existent in a long continuous furnace are usually controlled by conventional techniques and independent controllers offering simply an acceptable operation of the whole system. This paper describes the development of a multi-zone dynamical model for an industrial tunnel-type continuous furnace used in brick and tile production. The model is based on fundamental principles of heating process although a degree of empiricism has been introduced to model relationships where the real mechanisms are either too complex to be modeled or the corresponding differential equations can not be solved. An important objective of developing this model is to ensure that it can be used within a supervisory and control framework. The overall control task is to drive the process to the desired thermodynamic equilibriums and to regulate the temperature profile through the plant. The validity of the model is demonstrated by comparing the predicted results with the experimental data. Furnace's parameters estimation is carried out using industrial data and the model performance is illustrated through simulation studies.

Keywords: Industrial Furnaces, Heat process, System Modeling, Simulation

Presenting Author's biography

Stamatis Manesis received his Ph.D. from University of Patras, School of Engineering, Greece, in 1986. He is Associate Professor in Division of Systems & Control of the Electrical & Computer Engineering Dept. in the same university. In 1998-99 he was with the Industrial Control Centre of the Strathclyde University as academic visitor. He designed various Industrial Automation Systems for Hellenic Industries. He has published over 70 conference and journal papers. He has written 3 textbooks. His research is oriented on the introduction and use of the Intelligent Control concepts and tools in Industrial Systems. Main research interests: Industrial Control, Industrial Automation, Industrial Networks, Programmable Logic Controllers, Expert-Fuzzy Control Systems-Intelligent Controllers and SCADA Systems.



1 Introduction

Tunnel-type continuous furnaces are used in brick and tile production plants to fire the products at high temperatures of more than 1000°C. A main characteristic of these furnaces are their large dimensions with tunnel length usually greater than 100 m and tunnel cross section 15 m², divided in a number of thermal processing zones. The products travel through the tunnel, typically with a piecewise constant flow, and get subjected to this successive thermal processing. A brief review of the fundamental principles and applications of thermal systems control is given in [1], where the heat exchanging procedure is mainly treated.

System modeling and control is an important issue in industrial engineering applications and particularly in complicated thermal processes. Conventional approaches to system modeling need many assumed conditions and rely heavily on mathematical tools, such as differential equations, transfer function and so on, which emphasize the precision and exact description of each quantity involved. The use of these mathematical tools is suitable and well-applied only in simple or well-defined systems. However, when the system is complicated, these conventional approaches become less effective [2].

High reliability of furnace systems is a crucial factor in achieving high product yield. A good mathematical model of the system is required in order to implement a better control scheme. The model will have to include continuous and discrete dynamics, but may also be infinite dimensional, depending on whether the temperature and aerodynamic states are modeled as distributed or lumped parameter systems. The first step in the design of a model-based controller is the development of a thermal model which accurately captures the actual physical behavior of the system to be controlled. This high-fidelity thermal model is based on the application of the dynamic heat transfer equations to the system. The model may contain physical variables whose values are not known in advance (e.g. heat transfer coefficients) and are identified from experimental data. A comparison of the model response with the actual system output provides a measure of model accuracy.

In the last fifteen years, considerable amount of research has been reported on industrial furnaces modeling. A real-time furnace modeling and diagnostic approach has been developed in [3] for a multi-zone batch furnace used in semiconductor industry. The furnace system has been modeled based on both physical considerations and experimental data extraction using the electrical equivalent of the thermal process. The dynamic modeling of an industrial electric arc furnace is described in [4]. The main focus of this work involves the application of mathematical modeling techniques to develop a dynamic model of the furnace steel-making process.

The dynamic model of the hot section of an incineration plant with steam production is described in [5]. The hot section of the plant comprises a furnace, a postcombustion chamber and a boiler. The model is based on a first-principles approach that starting from material, energy, and momentum balances lead to the integration of a differential-algebraic system of 132 equations. A computational fluid dynamics modeling and simulation approach of an industrial continuous bread-baking process has been developed in [6]. The described two-dimensional model of the whole baking oven chamber facilitates a better understanding of the baking process and the unsteady heat transfer as well as the heating history and temperature distribution within dough/bread. A different kind of furnace, a rotary cement kiln is examined in [7], where a comprehensive one-dimensional model has been developed to simulate complex processes occurring inside kiln. The model is then used to understand the influence of various design and operating parameters on kiln performance. A PC-based process supervisory control and optimization software, called LINEMOD, combines advanced modeling with conventional control methods to monitor, control, and diagnose sintering furnaces or other thermal processes [8].

The modeling and control of distributed thermal systems is investigated in [9] where model-based control design techniques are applied. A dynamic model of reheating furnace based on fuzzy system and genetic algorithm is proposed in [2]. A basic goal in all research efforts concerning the control of tunnel-type furnace systems is the mathematical modeling of them as has been done in other classical types of furnaces [10, 11, 12]. The obtained models can be used efficiently for the analysis as well as for the synthesis of the control strategy of these furnace thermal systems.

Along a tunnel-type furnace there are several subsystems in operational interrelation which are responsible for the dominant thermal and aerodynamic states inside the furnace. According to a standard practice, in brick and tile manufacturing we use a series of single loop controllers in order to control these different subsystems. The control task is today performed with conventional PID controllers that provide an acceptable operation of the plant [13]. The PID controllers however cannot ensure that there is not deviation from the desirable operating points. This means that there are still significant open control problems; one such problem is the difference in temperature between the top and the bottom of the tunnel, despite the action of the air-recycling and side-burners subsystems. Furthermore, current operation is far from an optimal one from the energy consumption point of view. There are significant thermal losses and the fuel consumption can be substantially reduced. The paper proposes a model to be used exactly for solving the preceding problems. Attention has been

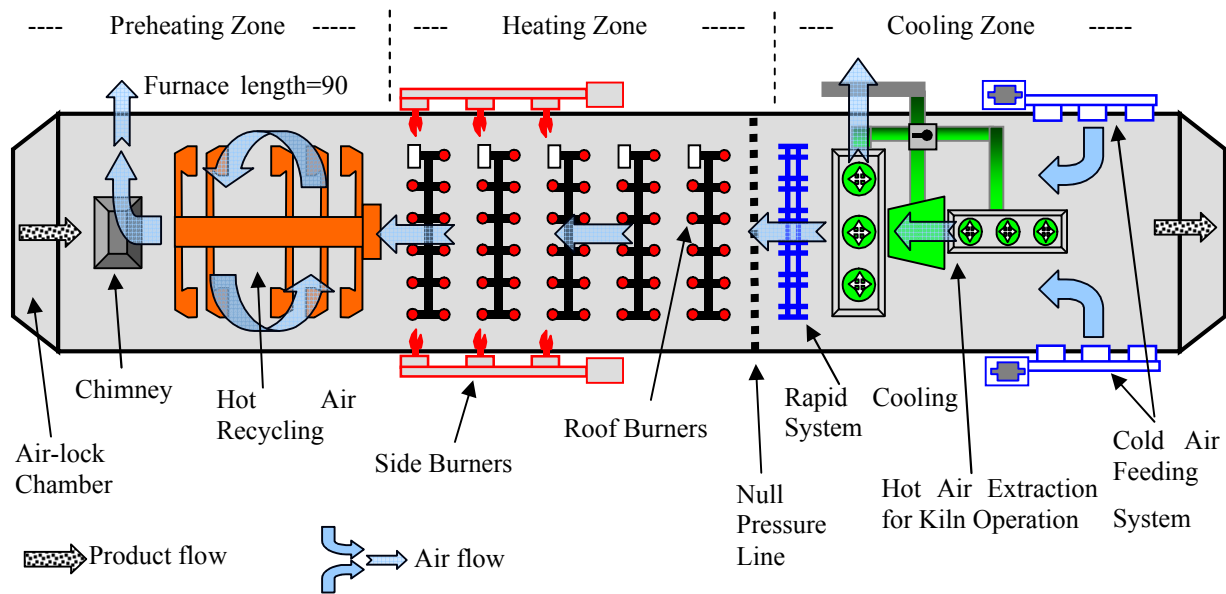


Fig. 1 Schematic overview of a tunnel-type furnace for brick and tile production

focused on a double purpose. On the one hand, the model must be a closed approximation to the real system and incorporate most of its salient features. On the other hand, must not be so complex that it is impossible to understand and experiment with it.

2 The tunnel-type continuous furnace for brick production

A tunnel-type industrial furnace consists of several subsystems in operational interrelation and is divided usually in three main zones, the pre-heating zone, the heating zone and the cooling zone as shown in Fig. 1. Two basic subsystems are responsible for the thermal and aerodynamic states created inside the furnace. The system's heart is the heating zone consisting of a matrix-set of burners. A typical number is eighty burner flames or more located on the roof of the furnace. In order to achieve isothermal distribution of heat from top to bottom, there are also side burners at each side of the furnace for rapid actions and temperature corrections. In some cases, the fuel used in these two burner-groups is different and the corresponding combustion modelling and control presents additional difficulties.

In some production processes, the products have to be dehydrated before entering the furnace. In such cases a parallel passive kiln operates with hot air from furnace. Hence, another subsystem is that of hot air extraction from the furnace and specifically from the cooling zone. The hot air flow is regulated in various points of the furnace either by on/off tampers or by analog position tampers performing mixing with environment air in order to keep hot air flow and temperature constant. Immediately after the heating zone, there is a small subsystem performing a rapid reduction of the temperature. Another subsystem with multiple air fans feeds cool air from the environment

at the end of the tunnel. To keep the tunnel temperature constant from top to bottom, in addition to the side burners, there is also a subsystem for recycling hot air before the heating zone. Finally, a chimney at the beginning of the tunnel forces exhaust emissions to the environment affecting so the overall aerodynamic state inside the furnace. Fig.2 illustrates

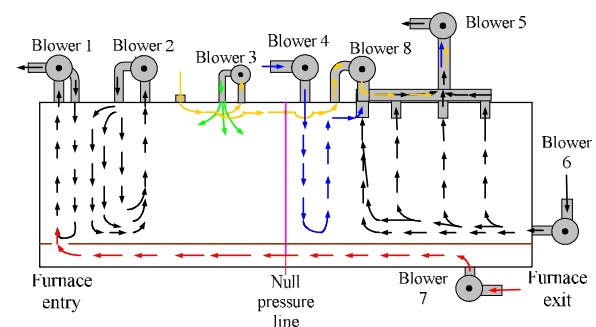


Fig. 2 Air flow pattern inside the furnace

the air flow inside the furnace caused by a set of blowers. Inside the preheating and heating zones there is hypo-pressure while in the cooling zone overpressure caused by the chimney blower and the cold air feeding system respectively. The point where the pressure is null, is called "null pressure line" and its control plays significant role in the operation of the furnace. The pressure distribution along the furnace is shown in Fig.3.

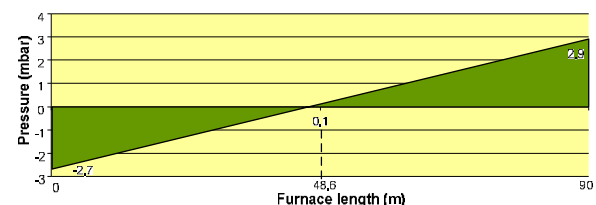


Fig.3 Diagram of air pressure along furnace

3 Physical model of thermal process

The tunnel-type industrial furnace is a very complex object for modeling and control, because multiple exchange of energy occurs in it due to the nature of process that leads to complex mathematical models describing its dynamics. In the past, tunnel-type industrial furnaces were often built with a central heating zone and thermal insulation that minimized heat loss through furnace walls. The result of such a design was to create an almost static system within the furnace from the aerodynamic point of view. A typical brick production process would involve placing a car of bricks inside the furnace, raising the temperature slowly to process temperature, holding for a specified time and then quickly cooling the furnace. While such processes are still common today, increasing demands for better temperature uniformity and greater yield are driving furnace makers to address complications related to the dynamics of the heating and cooling processes [9]. Today, furnace makers introduce forced multi-input multi-output air flow in order to achieve the desired temperature distribution across the furnace and to exploit as much as possible the heat losses in secondary zones.

3.1 Why modeling?

Before placing bricks inside the furnace, operators must determine optimum furnace settings (e.g. zone temperatures, cold air feeding, wagon insertion period) to ensure correct heat treatment of the bricks. Unfortunately, there is not a simple way to determine that the parts have attained the correct properties. One approach is to attach a probe to the bricks (in reality we need more than five probes because of the brick pallet dimensions) and constantly monitor property changes. This is feasible in a batch furnace with static parts, but presents insuperable difficulties with moving parts in a long continuous furnace. The technique is extremely time consuming and expensive involving inserting thermocouples in 32 wagons and recording temperature data as the wagons/bricks are moved through the furnace. An alternative method is to use a remote wireless device to gather temperature data. The technique is satisfactory at lower temperatures, but when the temperature exceeds 1000°C, the size of the insulation needed to protect the sensors makes it unsuitable for brick furnace application.

3.2 Model physics

The thermal efficiency of a fuel-fired furnace is usually expressed by the ratio of heat transfer to the load to the energy input in the fuel. There are three basic and interdependent mechanisms of heat transfer, the thermal radiation, convection and conduction. The steady-state energy balance is given by

$$\dot{Q}_G + \dot{Q}_{pa} = \dot{Q}_g + \dot{Q}_L + \dot{Q}_l \quad (1)$$

where \dot{Q}_G is the energy input supplied in the fuel,

\dot{Q}_{pa} is the rate of energy supply in preheated combustion air, \dot{Q}_g is the heat content of the flue products, \dot{Q}_L is the rate of heat transfer to the load and \dot{Q}_l expresses any kind of energy losses. The energy input supplied in the fuel is given by

$$\dot{Q}_G = \dot{V}_G C_V \quad (2)$$

where \dot{V}_G is the volumetric flow rate of fuel and C_V is the calorific value. The rate of energy supply in preheated combustion air is given by

$$\dot{Q}_{pa} = \dot{V}_G R_s (1 + X) \rho_a E_{th,a} \quad (3)$$

where R_s is the stoichiometric air/flow volume ratio, X is the percentage excess air level, ρ_a is the density of air at the reference temperature and pressure and $E_{th,a}$ is the specific enthalpy of the preheated air. Assuming complete combustion, the heat content of the flue products at temperature T_g is given by

$$\dot{Q}_g = \dot{V}_g (P_s + R_s X) \rho_g E_{th,g}(T_g) \quad (4)$$

where P_s is the combustion product/fuel volume ratio, ρ_g is the density of the combustion products and $E_{th,g}$ is the specific enthalpy of the combustion products as a function of temperature. Finally, assuming a process load throughput of \dot{b}_L , the rate of heat transfer to the load is given by

$$\dot{Q}_L = \dot{b}_L [E_{th}(T_o) - E_{th}(T_i)] \quad (5)$$

where $E_{th}(T_o)$ and $E_{th}(T_i)$ are the specific enthalpies of the load at the outlet and inlet temperature respectively.

The dominant mode of heat transfer from the flame and combustion products inside furnace is the non-luminous gaseous radiation. In fossil-fuel fired combustion processes, carbon dioxide and water vapor are the most important emitters of gaseous radiation. Carbon monoxide and methane also absorb and emit radiation, but they are usually absent or exist at very low concentrations. Thermal radiation transfer can occur from surfaces and gases within a tunnel-type furnace. All surfaces within industrial furnaces, emit, reflect and absorb radiation from their surroundings and thereby participate in the overall exchange of radiant energy to a load. For modeling a tunnel-type industrial furnace, we consider that all furnace surfaces are grey Lambert surfaces where emissivity is assumed to be independent of both wavelength and direction of radiation. For a grey Lambert surface the emissivity (ε) is equal to absorptivity (α) and $\varepsilon = 1 - \rho$, where ρ is the reflectivity coefficient. The energy transfer between two grey Lambert surfaces A_1 and A_2 of emissivities ε_1 and ε_2 respectively is given by

$$\dot{Q}_{1 \rightarrow 2} = (E_{b,1} - E_{b,2}) / \left[\frac{1}{A_1 \varepsilon_1} + \frac{1}{A_2} \left(\frac{1}{\varepsilon_2} - 1 \right) \right] \quad (6)$$

where E_b is the emissive energy of surface.

The gaseous atmosphere in any fuel-fired furnace participates in the overall interchange of radiation. A parallel beam of radiation passing through an absorbing grey gas is attenuated in proportion to its intensity and the distance traversed through the gas. The radiant emission from a volume V of gas at temperature T_g and with attenuation coefficient K is given by $\dot{Q} = 4\sigma KVT_g^4$ where σ is the Boltzman constant. When a beam of radiation is incident upon a particle, scattering occurs by diffraction, refraction and reflection. However, because the diameter of soot particles in gaseous and liquid fuel flames is usually quite small, scattering of radiation by soot may be considered negligible compared with emission and radiation. On the other hand, methods of calculating scatter and for predicting the scattering coefficient are dependent on the particle distribution/concentration and this information is difficult to obtain.

4 Multi-zone mathematical modeling

Most heating plant models are based on either the zone method for radiation analysis or the computational fluid dynamics models referred to in [14]. In multi-dimensional zone models, both longitudinal and cross-sectional or radial variations in temperature and heat flux are considered. Because of the large length (90 m) of the industrial furnace for brick and tile production, it is more convenient to consider the multi-zone model shown in Fig.4.

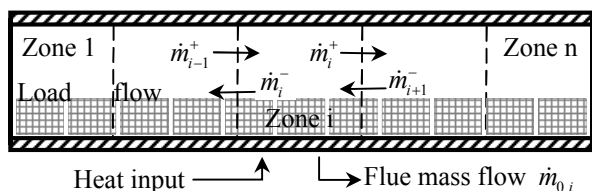


Fig.4 A long furnace model with recirculation between zones

According to multi-zone method, the furnace radiating enclosure is divided into isothermal volume and surface zones. A total energy balance is written over each zone in terms of the radiation arriving at it from all the zones in enclosure. Thus the radiant energy balance including radiation arriving at surface i is

$$\dot{Q}_i = \sum_{j=1}^n \overline{S_j S_i} E_{bj} + \sum_{j=1}^l \overline{G_j S_i} E_{gj} - A_i \varepsilon_i E_{bi} \quad (7)$$

where \dot{Q}_i is the energy flow to zone i , \overline{SS} and \overline{GS} are the exchange factors known as surface-surface and gas-surface directed flux areas respectively, E_g is the black body emissive power of a gas, n is the number

of surface zones and l is the number of volume zones. The geometry and input data for each volume and surface zone can be varied to match the specified design and operating conditions of the furnace. For a long-furnace model with fuel and air input to the specified zones shown in Fig.4, the flow of combustion products between zones is resolved into forward and reverse flow components \dot{m}^+ and \dot{m}^- respectively. The energy balance is then given by

$$\dot{Q}_{G,i} + \dot{Q}_{pa,i} + \dot{Q}_{th,i} - \dot{Q}_{co,i} - \dot{Q}_{ra,i} = 0 \quad (8)$$

where $\dot{Q}_{G,i}$ is given by Eq.(2) and $\dot{Q}_{pa,i}$ is the heat input in the combustion air given by Eq.(3). $\dot{Q}_{co,i}$ and $\dot{Q}_{ra,i}$ are the convective and radiative heat transfer from the combustion products to the surrounding surfaces in zone i respectively. $\dot{Q}_{th,i}$ is the flow of enthalpy to zone i in the combustion products and is given by

$$\begin{aligned} \dot{Q}_{th,i} = & \dot{m}_{i-1}^+ E_{th,g}(T_{g,i-1}) + \dot{m}_{i+1}^- E_{th,g}(T_{g,i+1}) - \\ & - [\dot{m}_i^- + \dot{m}_i^+ + \dot{m}_{0,1}] E_{th,g}(T_{g,i}) \end{aligned} \quad (9)$$

Also, the equation of air masses equilibrium must be valid in each zone

$$(\dot{m}_g)_i + (\dot{m}_a)_i + (\dot{m}_{i-1}^+) + (\dot{m}_{i+1}^-) - (\dot{m}^+ + \dot{m}^-)_i - (\dot{m}_0)_i = 0 \quad (10)$$

The above model is capable of simulating the effects of recirculation between zones (described in section 2) provided the forward and reverse flow components are specified. The solution of each volume zone energy balance equation is dependent on the combustion product temperatures in the neighboring zones. The equations for all volume zones must therefore be solved simultaneously in order to derive the zone temperature $T_{g,i}$.

In order to achieve a model being a close approximation of the physical process, the furnace has been divided into seven individual zones. The main preheating zone was considered as one modeling sub-zone because of its low temperature profile and small length (~16m). Each one of the main heating and cooling zones was divided into three sub-zones. The number (7) of sub-zones was selected aiming at low temperature variation inside each sub-zone and simultaneously at small number of differential equations. Since the constructing materials are different for side walls, roof surface, brick load, and wagons' floor surface, we have to consider four surfaces instead of two considered in section 3.2. First the modeling task requires to derive the temperatures of four surfaces at each sub-zone as a function of temperature of the sub-zone. Then, the energy conservation equations must be written for all sub-zones and solved simultaneously obtaining the various temperatures inside the corresponding sub-zones. As a

Tab.1 Physical properties of solids used in furnace construction

Raw Material	Emissivity Constant ε	Thermal Conductivity λ (W/mK)	Structural Element	Emissivity Constant ε	Convective Heat Transfer Coefficient h (W/m ² K)	Multi-layer Convective Heat Transfer Coefficient $\Sigma(\lambda_i/d_i)$ (W/m ² K)
Firebrick	0.72	1	Wall (w)	0.81	0.163	3.054
Perlite-Cement	0.9	0.085	Roof (r)	0.72	0.346	22.89
Ceramic Fiber Cloth	0.53	0.23	Wagon (c)	0.77	0.848	42.09
Concrete	0.92	1.25	Brick (b)	0.93	1.036	-
Brick	0.93	1.15				

d=layer thickness, i expresses the layer, (w,r,c,b)=meaning of subscripts in equations

matter of fact, walls and roof are not perfectly homogeneous. Since they are made of two or more layers of insulating materials, there are discontinuities passing from one layer to another due to thermal conductivity changes. Also, the floor of the furnace is formed with special multi-layer fire-resistant wagons. The various insulating raw-materials are firebrick, perlite and cement admixture, concrete, and ceramic fiber cloth. Tab. 1 summarizes the thermal properties of the raw-materials as well as of the multi-layer composite walls, roof, wagons floor, and brick load. The gas-surface and surface-surface directed flux areas as also the sub-zones' surfaces, listed in Tab.2, was calculated based on the dimensions of the furnace, wagon, brick pallet and sub-zone length. In order the model to take into account the energy transferred from

zone to zone by the flow of combustion products, we must know the quantities of air masses moved through zones. These are specified in Fig. 5. The last three sub-zones are missing since there are not burners and the null pressure line exists between fourth and fifth sub-zone. There are also special channels inside the furnace roof and floor for air cooling.

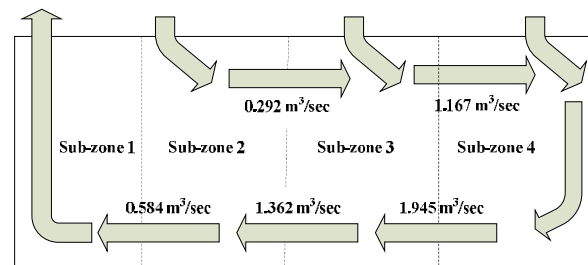


Fig. 5 The movement and quantities of air masses inside the first four sub-zones

Tab.2 Sub-zones' surfaces, S_iS_j and GS_j directed flux areas (m²), and external temperatures (°K)

Sub-Zone	1	2	3	4	5	6	7
A_w	69.7	34.8	46.5	46.5	46.5	69.7	58
A_r	72.9	36.5	48.6	48.6	48.6	72.9	60.8
A_c	31.9	15.9	21.3	21.3	21.3	31.9	26.6
A_b	317	158	211	211	211	317	264
S_bS_w	81.7	39.4	52.5	52.5	52.5	78.7	68
S_bS_r	66.8	32.3	43	43	43	64.6	55.7
S_bS_c	53.3	25.9	34.6	34.6	34.6	51.9	44.4
S_rS_w	18.8	8.99	11.9	11.9	11.9	17.9	15.7
S_wS_c	17.4	8.3	11.1	11.1	11.1	16.6	14.4
S_rS_c	16.1	7.73	10.3	10.3	10.3	15.4	13.4
GS_w	0	14.5	19.4	19.4	0	0	0
GS_r	0	12.4	16.6	16.6	0	0	0
GS_c	0	4.99	6.7	6.7	0	0	0
GS_b	0	93.5	124	124	0	0	0
T_{ew}	300	306	306	306	303	303	303
T_{er}	353	453	493	513	403	373	343
T_{ec}	298	313	313	313	308	303	298
T_{eb}	303	613	873	1023	1073	1023	793

Now, we can proceed to the modeling of each sub-zone separately. Because of the limited space, we present here only the model of the second sub-zone as an example.

4.1 2nd sub-zone model

From Eq.5 and Eq.7 we derive the equation of the energy behavior of the furnace walls

$$\begin{aligned} & \overline{GS}_w E_{g2} + \overline{S}_b \overline{S}_w E_{b2} + \overline{S}_r \overline{S}_w E_{r2} - A_{w2} \varepsilon_w E_{w2} + \\ & + A_{w2} h_w (T_{g2} - T_{w2}) - \\ & - A_{w2} (T_{w2} - T_{ew2}) \left[\sum (\lambda_i / x_i) \right]_w = 0 \end{aligned} \quad (11)$$

Similarly, the corresponding equations for the furnace roof and wagons are

$$\begin{aligned} & \overline{GS}_r E_{g2} + \overline{S}_b \overline{S}_r E_{b2} + \overline{S}_w \overline{S}_r E_{w2} - A_{r2} \varepsilon_r E_{r2} + \\ & + A_{r2} h_r (T_{g2} - T_{r2}) - A_{r2} (T_{r2} - T_{er2}) \left[\sum (\lambda_i / x_i) \right]_r \\ & - 0.33 \left[C_{PA80} \Pi_{Ar} P_{A80} (T_{ArOUT} - T_{ArIN}) \right] = 0 \end{aligned} \quad (12)$$

$$\begin{aligned} & \overline{GS}_c E_{g_2} + \overline{S}_b \overline{S}_c E_{b_2} - A_{c_2} \varepsilon_c E_{c_2} + \\ & + A_{c_2} h_c (T_{g_2} - T_{c_2}) - A_{c_2} (T_{c_2} - T_{ec2}) \left[\sum (\lambda_i / x_i) \right]_c \\ & - 0.19 \left[C_{PA40} \Pi_{Kc} P_{A40} (T_{AcOUT} - T_{AcIN}) \right] = 0 \quad (13) \end{aligned}$$

In preceding equations, C_{PA40} and C_{PA80} are the specific heats of the air at 40°C and 80°C respectively, Π_{Ar} and Π_{Kc} the air flows for roof and wagons cooling, P_{A40} and P_{A80} are the air densities at 40°C and 80°C respectively, T_{ArOUT} is the temperature of outlet air for roof cooling (80°C), T_{ArIN} is the temperature of inlet air for roof cooling (30°C), T_{AcOUT} is the temperature of the outlet air for wagons cooling (40°C), T_{AcIN} is the temperature of the inlet air for wagons cooling (25°C). The constants 0.33 and 0.19 express the percentage of energy losses due to roof and wagons cooling in the second sub-zone respectively. By substituting the above parameters in Eq.11-13 we derive the system of equations

$$\begin{aligned} & 14.56 \cdot \sigma \cdot T_{g_2}^4 + 39.36 \cdot \sigma \cdot 613^4 + 8.99 \cdot \sigma \cdot T_{r_2}^4 - \\ & - 28.18 \cdot \sigma \cdot T_{w_2}^4 + 5.67 (T_{g_2} - T_{w_2}) - 106.27 (T_{w_2} - 306) = 0 \\ & 12.47 \cdot \sigma \cdot T_{g_2}^4 + 32.3 \cdot \sigma \cdot 613^4 + 8.99 \cdot \sigma \cdot T_{w_2}^4 - 115.46 \\ & - 26.28 \cdot \sigma \cdot T_{r_2}^4 + 12.62 (T_{g_2} - T_{r_2}) - 835.48 (T_{r_2} - 453) = 0 \\ & 4.99 \cdot \sigma \cdot T_{g_2}^4 + 25.92 \cdot \sigma \cdot 613^4 - 12.24 \cdot \sigma \cdot T_{c_2}^4 + \\ & + 13.48 (T_{g_2} - T_{c_2}) - 669.23 (T_{c_2} - 313) - 17931 = 0 \end{aligned}$$

which has been solved using Mathematica 5.0. The solution of the system gave the internal surface temperatures T_{w_2} , T_{r_2} , T_{c_2} as functions of the sub-zone temperature T_{g_2} . Since it is impossible to include these long equations, let call them “internal temperature equations” for understanding purposes. The application of the energy conservation equation (Eq.8) in the second sub-zone implies

$$\begin{aligned} & \dot{V}_{G2} [CV_{net} + R_S (1 + X/100) \rho_a^o (H_a (T_{ArOUT}))] + \\ & + \dot{m}_3^- H_g (T_{g_3}) - \dot{m}_2^- H_g (T_{g_2}) - \dot{m}_2^+ H_g (T_{g_2}) - \\ & - A_{b_2} h_b (T_{g_2} - T_{b_2}) - A_{w_2} h_w (T_{g_2} - T_{w_2}) - \\ & - A_{r_2} h_r (T_{g_2} - T_{r_2}) - A_{c_2} h_c (T_{g_2} - T_{c_2}) - \\ & - (\overline{GS}_b E_{g_2} + \overline{GS}_w E_{g_2} + \overline{GS}_r E_{g_2} + \overline{GS}_c E_{g_2}) + \\ & + (\overline{GS}_b E_{b_2} + \overline{GS}_w E_{w_2} + \overline{GS}_r E_{r_2} + \overline{GS}_c E_{c_2}) = 0 \quad (14) \end{aligned}$$

4.2 Overall model for seven sub-zones

Continuing the modeling of the second sub-zone it would be supposed to substitute the “internal temperature equations” into Eq.14 to obtain one new equation with two unknown variables, the

temperatures T_{g_1} and T_{g_2} . Performing the same procedure for all sub-zones, we would lead to a system of seven equations with seven unknown variables T_{g_1}, \dots, T_{g_7} . Because of the complex form of the “internal temperature equations”, the system of seven equations is unsolvable even with the today best software tools for solving equations. Instead, it is possible to determine the arithmetic values of the internal temperatures T_w , T_r and T_c in each sub-zone using the real values of sub-zones’ temperatures T_{g_1}, \dots, T_{g_7} , which will correspond to a perfect operation of the plant. By substituting the arithmetic values of T_w , T_r and T_c in energy conservation equations (similar to Eq.14), the system of seven equations will be solvable. Then, it will remain to validate the model that means to examine the agreement between the simulated and the measured temperatures of the sub-zones.

Performing the same procedure presented in section 4.1 for all sub-zones, we derive the following solvable system of seven equations with seven unknowns variables the sub-zones’ temperatures,

$$\begin{aligned} & \dot{m}_2^- H_g (T_{g_2}) - \dot{m}_1^- H_g (T_{g_1}) - \\ & - A_{b_1} h_b (T_{g_1} - T_{b_1}) - A_{w_1} h_w (T_{g_1} - T_{w_1}) - \\ & - A_{r_1} h_r (T_{g_1} - T_{r_1}) - A_{c_1} h_c (T_{g_1} - T_{c_1}) = 0 \quad (15) \end{aligned}$$

$$\begin{aligned} & \dot{V}_{G2} [CV_{net} + R_S (1 + X/100) \rho_a^o (H_a (T_{ArOUT}))] + \\ & + \dot{m}_3^- H_g (T_{g_3}) - \dot{m}_2^- H_g (T_{g_2}) - \dot{m}_2^+ H_g (T_{g_2}) - \\ & - A_{b_2} h_b (T_{g_2} - T_{b_2}) - A_{w_2} h_w (T_{g_2} - T_{w_2}) - \\ & - A_{r_2} h_r (T_{g_2} - T_{r_2}) - A_{c_2} h_c (T_{g_2} - T_{c_2}) - \\ & - (\overline{GS}_b E_{g_2} + \overline{GS}_w E_{g_2} + \overline{GS}_r E_{g_2} + \overline{GS}_c E_{g_2}) + \\ & + (\overline{GS}_b E_{b_2} + \overline{GS}_w E_{w_2} + \overline{GS}_r E_{r_2} + \overline{GS}_c E_{c_2}) = 0 \quad (16) \end{aligned}$$

$$\begin{aligned} & \dot{V}_{G3} [CV_{net} + R_S (1 + X/100) \rho_a^o (H_a (T_{ArOUT}))] + \\ & + \dot{m}_4^- H_g (T_{g_4}) - \dot{m}_3^- H_g (T_{g_3}) - \dot{m}_3^+ H_g (T_{g_3}) + \\ & + \dot{m}_2^+ H_g (T_{g_2}) - \\ & - A_{b_3} h_b (T_{g_3} - T_{b_3}) - A_{w_3} h_w (T_{g_3} - T_{w_3}) - \\ & - A_{r_3} h_r (T_{g_3} - T_{r_3}) - A_{c_3} h_c (T_{g_3} - T_{c_3}) - \\ & - (\overline{GS}_b E_{g_3} + \overline{GS}_w E_{g_3} + \overline{GS}_r E_{g_3} + \overline{GS}_c E_{g_3}) + \\ & + (\overline{GS}_b E_{b_3} + \overline{GS}_w E_{w_3} + \overline{GS}_r E_{r_3} + \overline{GS}_c E_{c_3}) = 0 \quad (17) \end{aligned}$$

$$\begin{aligned} & \dot{V}_{G4} [CV_{net} + R_S (1 + X/100) \rho_a^o (H_a (T_{ArOUT}))] - \\ & - \dot{m}_4^- H_g (T_{g_4}) + \dot{m}_3^+ H_g (T_{g_3}) - \\ & - A_{b_4} h_b (T_{g_4} - T_{b_4}) - A_{w_4} h_w (T_{g_4} - T_{w_4}) - \\ & - A_{r_4} h_r (T_{g_4} - T_{r_4}) - A_{c_4} h_c (T_{g_4} - T_{c_4}) - \\ & - (\overline{GS}_b E_{g_4} + \overline{GS}_w E_{g_4} + \overline{GS}_r E_{g_4} + \overline{GS}_c E_{g_4}) + \end{aligned} \quad (18)$$

$$\begin{aligned}
&+(\overline{GS}_b E_{b4} + \overline{GS}_w E_{w4} + \overline{GS}_r E_{r4} + \overline{GS}_c E_{c4}) = 0 \\
&-A_{b5} h_b (T_{g5} - T_{b5}) + A_{w5} h_w (T_{g5} - T_{w5}) + \\
&+ A_{r5} h_r (T_{g5} - T_{r5}) - A_{c5} h_c (T_{g5} - T_{c5}) - \\
&-[C_{PA170} \Pi_{AF} P_{A800} (T_{AFOUT} - T_{AFIN})] * 0.35 - \\
&-[C_{PA170} \Pi_{RC} P_{A800} (T_{RCOUT} - T_{RCIN})] = 0
\end{aligned} \quad (19)$$

$$\begin{aligned}
&-A_{b6} h_b (T_{g6} - T_{b6}) + A_{w6} h_w (T_{g6} - T_{w6}) + \\
&+ A_{r6} h_r (T_{g6} - T_{r6}) - A_{c6} h_c (T_{g6} - T_{c6}) - \\
&-[C_{PA170} \Pi_{AF} P_{A650} (T_{AFOUT} - T_{AFIN})] * 0.35 = 0
\end{aligned} \quad (20)$$

$$\begin{aligned}
&-A_{b7} h_b (T_{g7} - T_{b7}) + A_{w7} h_w (T_{g7} - T_{w7}) + \\
&+ A_{r7} h_r (T_{g7} - T_{r7}) - A_{c7} h_c (T_{g7} - T_{c7}) - \\
&-[C_{PA170} \Pi_{AF} P_{A400} (T_{AFOUT} - T_{AFIN})] * 0.2 = 0
\end{aligned} \quad (21)$$

where Π_{AF} , Π_{RC} , T_{AFOUT} , T_{AFIN} , T_{RCOUT} and T_{RCIN} are quantities similar to these described in Eq.13 but for the cold air feeding system (AF) and the rapid cooling system (RC) respectively. Based on Eq.15-21 we can verify the operation of the furnace, predict the behavior of the system at boundary conditions and finally determine the rate of energy losses through the furnace surfaces.

5 Simulation results and discussion

Typical goals of a supervisory controller are safe operation, highest product quality, and most economic operation. All three goals are usually impossible to achieve simultaneously, so they must be prioritized. The temperature along the whole length of the tunnel must follow a predefined curve depending on the kind of the process. For example, in very long furnaces for

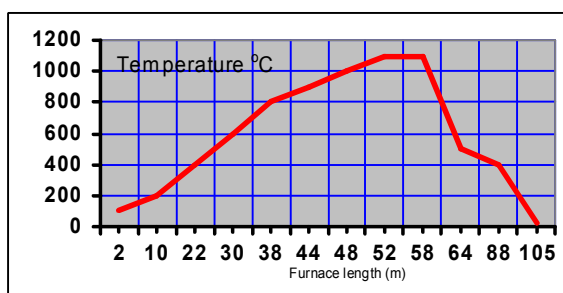


Fig. 6 Furnace temperature profile.

conventional ceramic products, the temperature profile must follow the one depicted in Fig. 6. As mentioned above, there is a forced inlet of air at the end of the furnace while there is a forced outlet at the beginning of the furnace. The difference in pressure results in a net flow of air from one end to the other. In addition to controlling the temperature of the furnace, one has

also to regulate and control the stability of this aerodynamic state. The null pressure line must lie in a constant location between the heating and cooling zone. A possible shifting of null-pressure line in the heating zone means that cool air enters the heating zone which is forbidden. On the other hand, a possible shifting in the cooling zone implies that exhaust emissions will enter the kiln, which is also undesirable. To keep the null-pressure line constant, there must be a continuous control of the cool air inlet flow. The chimney flow is treated as a disturbance, since it varies independently to keep exhausts temperature at a low level for saving energy.

5.1 Simulation results

Each set of “internal temperature equations” concerning the corresponding sub-zone can be simulated as a function of the sub-zone’s temperature. It is obvious, that for each triple $\{T_{wi}, T_{ri}, T_{ci}\}$ the sub-zone temperature T_{gi} varies inside a relatively narrow region of values, which is different for each sub-zone. However, in order to have a comparable illustration of the seven temperatures on the same diagram, the simulation has been performed for T_g between 270°K and 1400°K, as shown in Fig.7-9. Doing so, it is

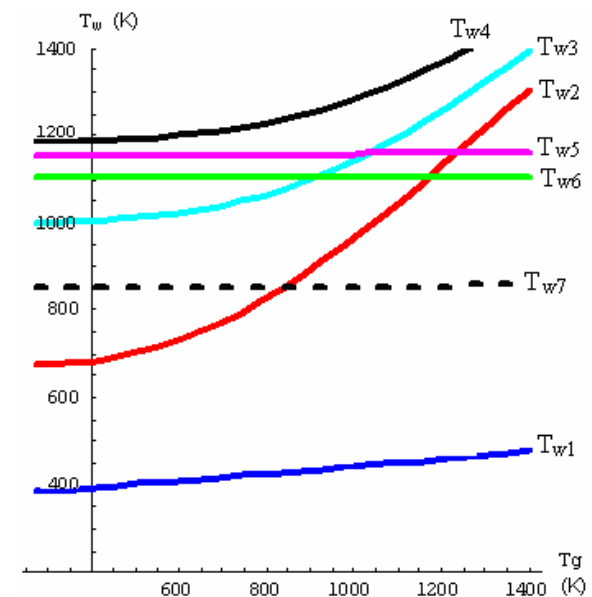


Fig. 7 The internal temperature of walls (T_w) in all sub-zones.

possible to derive some general consequences about the temperature behaviour of the three different surfaces along the furnace. It can be seen from the trends of Fig.7 that the temperature T_{w1} is low with a small increasing rate as T_g also increases. In the second sub-zone, the temperature T_{w2} presents a high increasing rate as T_g increases. This fact is reasonable and expected since in this sub-zone there are side burners. In third and fourth sub-zones, it is possible to observe a similar increment of T_{w3} and T_{w4} because of the roof burners. Passing in the cooling sub-zones, the temperatures T_{w5} and T_{w6} are high as the side walls

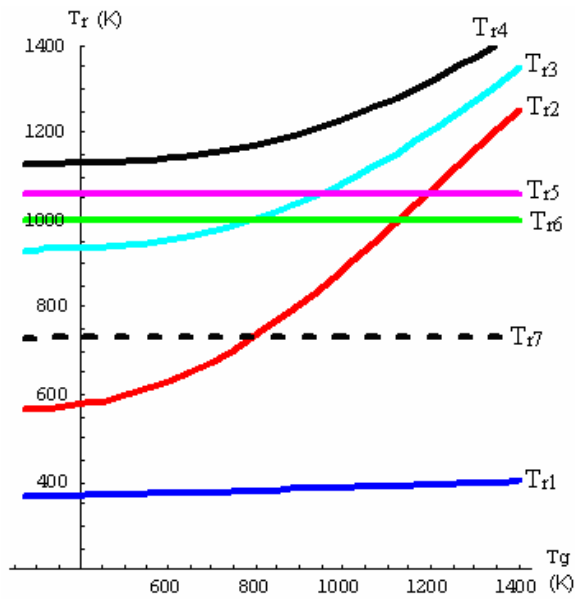


Fig. 8 The internal temperature of roof (T_r) in all sub-zones.

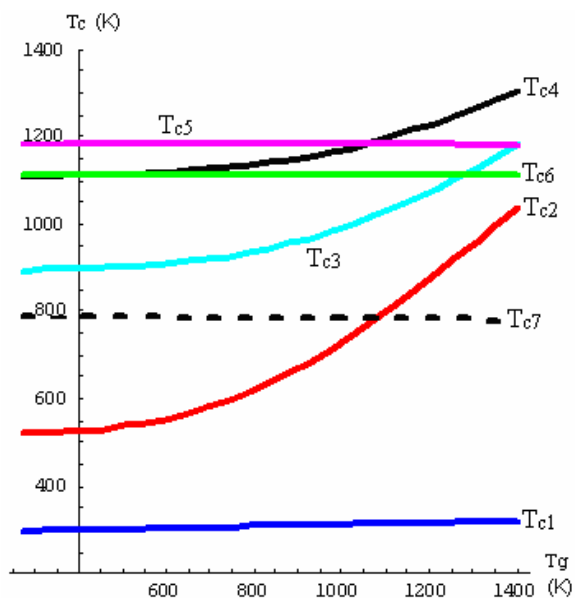


Fig. 9 The internal temperature of wagons (T_c) in all sub-zones.

absorb the thermal energy of bricks which are just coming out from the heating zone. T_{w5} and T_{w6} remain almost constant independently of the T_g variation. This means that the side walls have stored large amounts of thermal energy so that the T_g variation does not affect their temperature. The same performance presents the temperature T_{w7} in the last sub-zone but in a lower level. Similar consequences can be derived from the temperature trends T_{ri} and T_{ci} in Fig.8-9 respectively. The measured values of temperatures T_{g1}, \dots, T_{g7} which correspond to the desired operation of the furnace and will be used for the iterative calculation of the internal temperatures T_w, T_r, T_c in each sub-zone, are shown in Tab.3. The computation procedure includes the following steps,

Tab.3 Desired temperatures values in the center of sub-zones ($^{\circ}\text{K}$).

T_{g1}	T_{g2}	T_{g3}	T_{g4}	T_{g5}	T_{g6}	T_{g7}
550	830	1020	1100	1020	840	520

Step1: Using the $T_{gi}^{(0)}$, $i=1, \dots, 7$ values of Tab.3 solve the system of “internal temperatures equations” and calculate the internal surface temperatures $T_{wi}^{(0)}$, $T_{ri}^{(0)}$ and $T_{ci}^{(0)}$, $i=1, \dots, 7$.

Step2: By substituting the arithmetic values $T_{wi}^{(0)}$, $T_{ri}^{(0)}$ and $T_{ci}^{(0)}$, $i=1, \dots, 7$ of step1 into Eq.15-21, calculate the sub-zone temperatures $T_{gi}^{(1)}$, $i=1, \dots, 7$ that generally are different from the corresponding $T_{gi}^{(0)}$, $i=1, \dots, 7$.

Step3: Repeat steps 1 and 2 until to achieve the convergence of the values $T_{gi}^{(n-1)}$ and $T_{gi}^{(n)}$, $i=1, \dots, 7$,

where n is the number of iterations.

As shown in Fig.10, only a few iterations are needed in order to reach the convergence of the solutions for the first four sub-zone temperatures. The same is also valid for the other three temperatures. It can be seen also that, in all cases, the temperatures T_{gi} approach rapidly the steady state solution just from the second iteration.

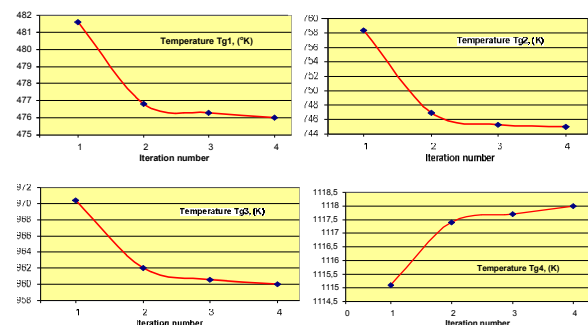


Fig.10 Iterative convergence of the calculated temperatures T_{g1}, T_{g2}, T_{g3} and T_{g4} .

The model simulation results are summarized in Tab.4 for all sub-zones whereas the furnace internal temperatures trends (measured and simulated) are shown in Fig.11. The effectiveness of the described

Tab.4 Measured and model-based values

	Measured values ($^{\circ}\text{K}$)	Simulated values ($^{\circ}\text{K}$)
T_{g1}	550	476
T_{g2}	830	745
T_{g3}	1020	960
T_{g4}	1100	1118
T_{g5}	1020	991
T_{g6}	840	822
T_{g7}	520	515

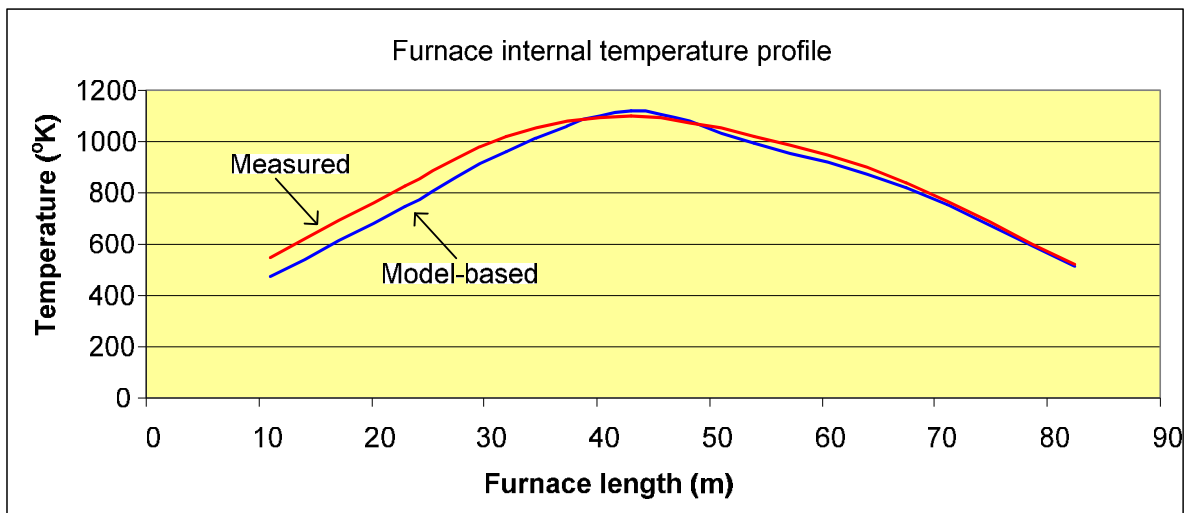


Fig.11 Comparison of experimental data and model simulation results.

model in simulating the behavior of the actual furnace process can be evaluated by comparing the measured temperature profile with the simulated temperature profile as shown in Fig.11. In general, the pattern of the model predicted temperature profile agrees well with that of the measured one. However, there is still discrepancy between the modeled profile and the measured experimental data. Tab.4 shows that there is a deviation of 70-80°K in the first two sub-zones and 60°K in the third one. The deviation in the fourth sub-zone is only 10°K indicating a general reduction of the difference as we are passing from the first sub-zone to the next ones. In the fourth sub-zone with the small deviation, the thermal energy source is mainly the fuel combustion whereas in the first sub-zone with the large deviation the only energy source is the circulated hot air. Presumably, the reason for the reduced agreement is the modeling of the hot air source and it will concentrate our effort for improvement of the model. In the last three sub-zones the deviation varies between 5 and 30°K that is quite low and actually such a difference is considered negligible by process operators. It is worth to point out that it is unrealistic to aim to reproduce exactly the experimental temperature profile. The existent agreement with experimental data shown by the described model allows consideration of it as a sound candidate for model-based control.



Fig. 12 Overview of the roof burners.

5.2 Model-based supervisory control

The desirable temperature profile succeeded mainly by the matrix-set of roof burners, shown in Fig. 12, is strongly affected by the convenient or no operation of the overall air flow system. From the introductory description in section 5, it is obvious that the supervisory control system using the developed model has to perform continuous control of various physical variables such as temperature, air flow and stoichiometric combustion, and discrete control (ON/OFF) of various dampers, burners, fans and doors. Most industrial furnaces are controlled using classical control algorithms such as ON-OFF or PID controllers. The popularity of PID control can be attributed to both its good performance over a wide range of operating conditions and to its functional simplicity. A common problem with PID controllers used for control of highly nonlinear processes is that the set of controller parameters produces satisfactory performance only when the process is within a small operational window. Outside this window, other parameters or set points are necessary, and these adjustments may be done automatically by a high level strategy. A supervisory system is a system that evaluates whether local controllers satisfy prespecified performance criteria, diagnoses causes for deviation from the performance criteria, plans actions, and executes the planned actions. For high level control and supervisory control several simple controllers can be combined in a priority hierarchy. The applied control system with supervisory controller consists of two hierarchical levels as shown in Fig. 13. The controller regulates the operation of burners based on the measurement of air flow inlet and temperature, and on the stoichiometric analysis data. The dependency of combustion instability on fuel mean velocity is strong and suggests that the dominant mechanism causing combustion instability is hydrodynamics and its interaction with flame. The proposed supervisory control scheme, based on the developed model, has

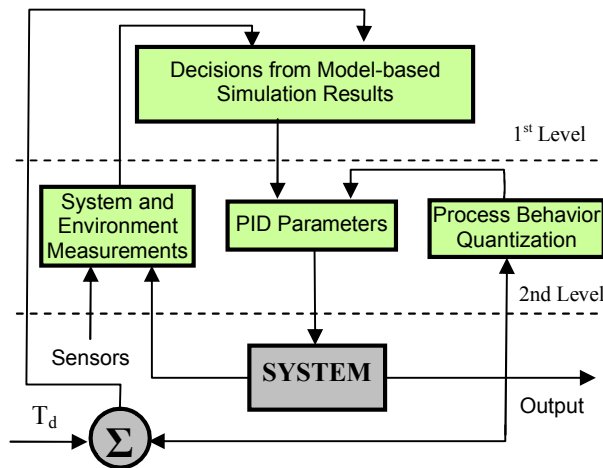


Fig.13 Hierarchical supervisory structure.

been tested with experimental data obtained from a 250 ton/24 hour brick furnace in Greece. Fig. 14 shows typical temperature variations at the top and the bottom of the tunnel furnace without the use of the model and action of the supervisory controller. Fig. 15 shows the reduction of the temperature difference between the top and the bottom of the tunnel obtained after the action of the supervisory controller.

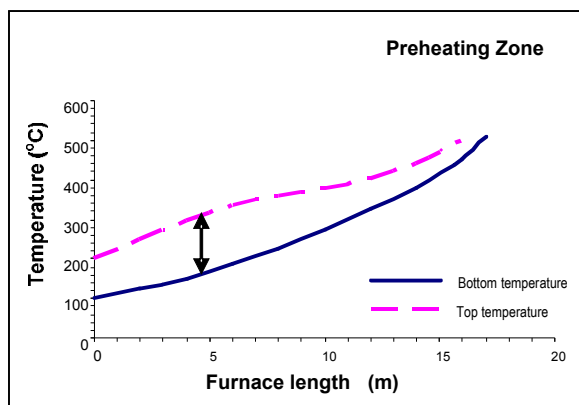


Fig. 14 Temperature variation along the furnace at the top and the bottom without supervisory control.

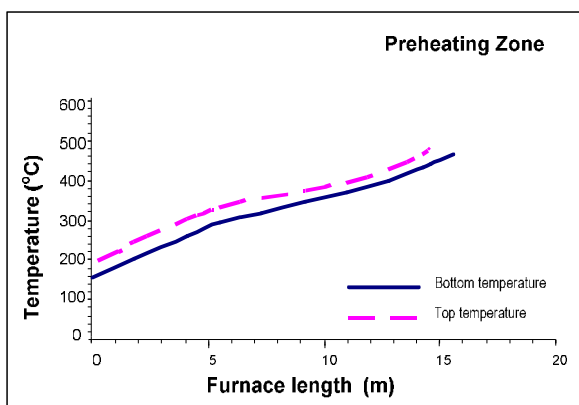


Fig. 15 Temperature difference of Fig. 6 after the action of the supervisory controller.

6 Conclusions

In this work, the industrial furnace system for brick production has been modeled based on both physical considerations and experimental data extraction. The model tries to combine both the computation simplicity and the capability of producing a good prediction of the system behaviour. In general, the simulated temperature profiles are satisfactory, despite the still-existed discrepancies between the experimental and modelled data. The model has been used to build a two-level supervisory control scheme. In addition, it forms a basis for future work including optimization of the process variables and implementation of an intelligent on-line control system.

7 References

- [1] M. Sen. A review of the principles and applications of thermal control. *Journal of the Mexican Society of Mechanical Engineering*, 1:115-131, 2004.
- [2] B. Zhang, L. Wang and H. Shao. Dynamic model of reheating furnace based on fuzzy system and genetic algorithm. *Proceedings of the American Control Conference*, 5:3823-3828, 2002.
- [3] J. Wang and C. Spanos. Real-time furnace modeling and diagnostics. *IEEE Transactions on Semiconductor Manufacturing*, 15:393-403, 2002.
- [4] R. MacRosty and C. Swartz. Dynamic modelling of an industrial electric arc furnace. *Industrial & Engineering Chemistry Research*, 44:8067-8083, 2005.
- [5] D. Manca and M. Rovaglio. Numerical modelling of a discontinuous incineration process with on-line validation. *Industrial & Engineering Chemistry Research*, 44:3159-3177, 2005.
- [6] S. Wong, W. Zhou and J. Hua. CFD modelling of an industrial continuous bread-baking process involving U-movement. *Journal of food Engineering*, 78:888-896, 2007.
- [7] K. Mujumdar, A. Arora and V. Ranade. Modeling of rotary cement kilns: applications to reduction in energy consumption. *Industrial & Engineering Chemistry Research*, 45:2315-2330, 2006.
- [8] H. Nandi and W. Ruhe. On-line modelling and new generation of supervisory control system for sintering furnaces. *CompAS Controls Inc. Indiana, USA*, 2002.
- [9] A. Naeni, J. Ebert, D. Roover, R. Kosut, M. Dettori, L. Porter and S. Ghosal. Modeling and control of distributed thermal systems. *IEEE Transactions on Control Systems Technology*, 11:668-683, 2003.

- [10] S. Pal and A. Lahiri. Mathematical model of COREX melter gasifier: Part II, Dynamic Model. *Metallurgical and Materials Transactions B*, 34B:115-121, 2001.
- [11] D. Debelikovic, I. Buzurovic, M. Rancic and S. Sarbon. Mathematical model of the pulverising plant as a mass accumulator with associated dynamics of both impeller and coal drying process. *Scientific Journal Facta Universitatis Mechanical engineering*, 1:653-664, 1999.
- [12] Q. He, S. Qin and A. Torpac. Computationally efficient modeling of wafer temperatures in an LPCVD furnace. *Journal on Advanced Process Control and Automation*, 5044:97-108, 2003.
- [13] S. Martineau, K. Burnham, O. Haas, G. Andrews and A. Heeley. Four-term bilinear PID controller applied to an industrial furnace. *Control Engineering Practice*, 12:457-464, 2004.
- [14] J. Rhine and R. Tucker. *Modeling and Control of Gas-Fired Furnaces and Boilers*. McGraw-Hill, 1991.